Characterizing unexpected slowing of the Cross Polar Jet over Alaska in the midnight sector

Rajan Itani, Mark Conde, John Elliott

Geophysical Institute, University of Alaska Fairbanks

Abstract

We have studied the auroral zone thermospheric winds in the midnight local time sector, using ground based optical Doppler spectroscopy of the 630 nm emission from atomic oxygen at around 240 km altitude. One of the most prominent recurring features seen in winds at these latitudes is the cross-polar jet emerging from the polar cap at local times around magnetic midnight. The standard view is that wind flows anti-sunward in the midnight sector, and spills equatorward over magnetic latitudes extending well below those of the auroral zone. The purpose of this study is to show that the existing view is too simplistic. At the magnetic latitudes of our observatory at Poker Flat, Alaska (~65 degrees), the anti-sunward flow is frequently seen to stall without spilling further equatorward. This behavior is most prevalent during low solar activity at mid-winter, when the combination of pressure gradient established by solar heating and the ion drag are not enough to allow the jet to push through the background atmosphere on the night side. At higher latitudes, by contrast, the flow is relatively uniformly anti-sunward around magnetic midnight (as expected in the polar cap), even during quiet conditions. During periods of higher solar and magnetic activity, the cross polar jet does spill equatorward over Alaska in the midnight sector as expected. This is a very significant large-scale difference between model predictions and the behavior that is actually observed, with potentially major ramifications – which is the motivation for the present study.

Introduction

Various techniques have been used over many years to measure the high latitude thermospheric wind circulation. One of the most productive has been measurement of the Doppler shift of naturally occurring atmospheric optical emissions by the use of Fabry-Perot Interferometer (FPI) . Low and mid latitude F-region thermospheric wind is mainly driven by the pressure gradients caused by the absorption of extreme ultraviolet solar radiation, with resultant steady-state winds being balanced by a combination of ion-drag and viscous drag. By contrast, ion-drag between neutral and plasma flow is the dominant source of momentum driving winds at high latitudes. Solar heating creates a high temperature region located near the subsolar point which, in turn, creates the day to night pressure difference. This accelerates the neutral wind until it is balanced by the ion-drag, viscosity and, in the lower thermosphere, the Coriolis force.

Various wind models as well as previous studies suggest that high latitude thermospheric winds form a “cross polar jet” that emerges from the polar cap in the midnight sector and spills further equatorward. Even though the cross polar jet is a well formed and powerful, flow feature, it appears to stall surprisingly easily upon leaving the polar latitudes. This phenomenon is frequent during solar minima but less common during solar maxima.

Here we have analyzed spectra of the 630 nm atomic oxygen emission to derive estimates of winds at around 240 km altitude. This well-known “red line” emission is a reliable indicator of the F-region of thermosphere because, although it spans a wide and somewhat variable range of altitudes, vertical gradients of the wind field are typically weak at heights above 200 km.

Instruments and Methods

The Scanning Doppler Imager (SDI) is an all-sky imaging Fabry-Perot Interferometer. The instrument and observing techniques are described by Conde and Smith [1995, 1997, 1998]. SDIs resolve the visible sky into a software-defined set of sub-regions, and compile a high resolution Doppler spectrum of the airglow/auroral emission for each sub-region. The current version of the instrument typically resolves the field-of-view into 115 sub-regions termed ‘zones’ as per the techniques described by Conde and Smith [1997]. These spectra are then used to infer Doppler line of sight (LOS) wind measurements and Doppler temperatures, as described by Conde et al. [2001]. Several methods currently are employed utilizing these LOS observations to infer three component wind fields at the height of atmospheric optical emission layer. Here we present results based on the simple “monostatic” wind fitting algorithm described by Conde & Smith [1998].

References

1. Conde, M., and Smith R. W., Mapping thermospheric winds in the Auroral zone, *Geophys. Res. Lett.*, 22, 3019-3022, 1995.
2. Conde, M., and Smith, R. W., Phase compensation of a separation scanned, all-sky imaging Fabry-Perot spectrometer for Auroral studies, *Appl. Opt.*, 36, 5441-5450, 1997.
3. Conde, M., and Smith, R. W., Spatial structure in the thermospheric horizontal wind above Poker Flat, Alaska, during solar minimum, *J. Geophys. Res.*, 103, 9449– 9471, 1998.
4. Conde, Craven, Immel, Hoch, Stenbaek-Nn, Hallinan, Smith, Olson, Wei Sun, Frank, and Sigwarth, Assimilated observations of thermospheric winds, the aurora, and ionospheric currents over Alaska, *J. Geophys. Res.*, 106:10493-10508, 2001.
5. Anderson, C. (2011), Optical Remote Sensing of Local-Scale Thermospheric Dynamics Above Antarctica, *Ph. D. thesis*, La Trobe University, Bundoora VIC, 3086 Australia, February 2011.
6. http://optics.gi.alaska.edu/realtime/data/PKR_DMSP/Keo_15hr/Keo_15hr/
7. ftp://ftp.ngdc.noaa.gov/STP/GEOMAGNETIC_DATA/INDICES/KP_AP
8. https://ccmc.gsfc.nasa.gov/requests/GetInput/get_indices.php

Acknowledgement

This work was supported by NSF award number 1452333, "CEDAR: High-resolution Multistatic Mapping of Small-Scale Flow Structures in Earth’s Auroral Thermosphere."

Results

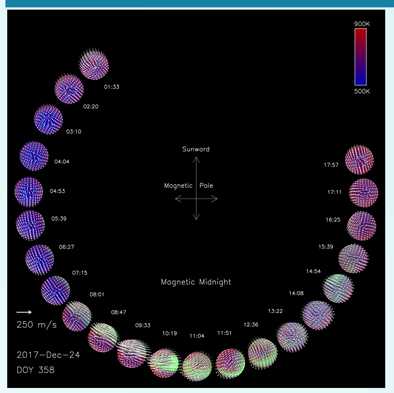

Figure 1: Maps of F-region neutral winds and temperature inferred from all-sky Doppler spectra of 630.0 nm atomic oxygen emission recorded at Poker Flat, Alaska for the night of 12/24/2017. We refer this as a typical wind dial plot. Blue through red colors depict the temperatures, derived from the spectrum in each zone, according to the color scale bar at the upper right corner. Green hue depict the intensity of 630.0 nm emission. The white arrows depict the wind vector, magnitude of which is as defined by the scale.

In Figure 2 we can see the anti-sunward flow of wind in the magnetic midnight sector and emerging across the polar cap and spilling equatorward. However in Figure 3, in the magnetic midnight sector we can see that the equatorward flow stalling at roughly the latitude of Poker Flat. This is an unexpectedly sudden and change in the large-scale flow (occurring over a few hundred km), that is not predicted by first-principles models.

Figure 4 and 5 show the example keogram for the two event types i.e.; emergent and stalled. We can see that the emergent event corresponds to the high Auroral activity.

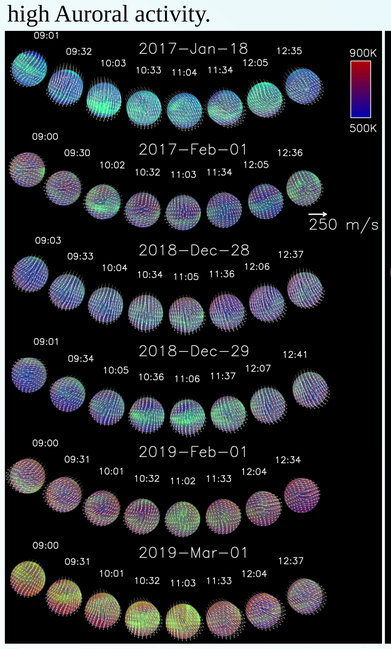

Figure 2: Midnight sector of wind-dial plots stacked together for the emergent events.

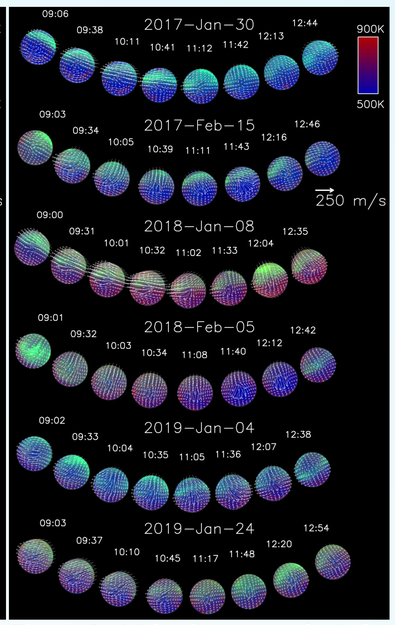

Figure 3: Midnight sector of wind-dial plot stacked together for all the stalled events.

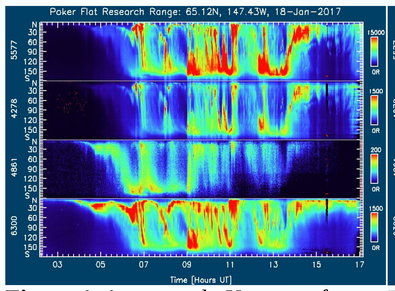

Figure 4: An example Keogram for the night of 1-18/2017 (active night)

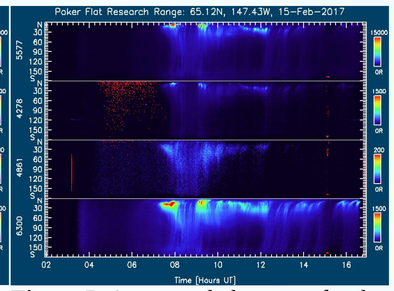

Figure 5: An example keogram for the night of 2-15-2017 (stalled event).

Figure 6 and 7 show the time series of fluctuations in the magnetic H-component recorded at Poker Flat, Alaska. Magnetic H perturbations were more active on the days corresponding to the emergent event when the cross polar jet spilled equatorward. However during the days when the wind seem stalled, fluctuations on magnetic H-component were conspicuously weaker.

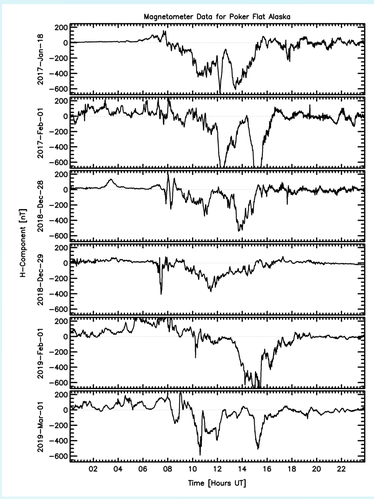

Figure 6: Time series of perturbations in the H-component of magnetic fields recorded at Poker Flat Alaska for the emergent events, during six days.

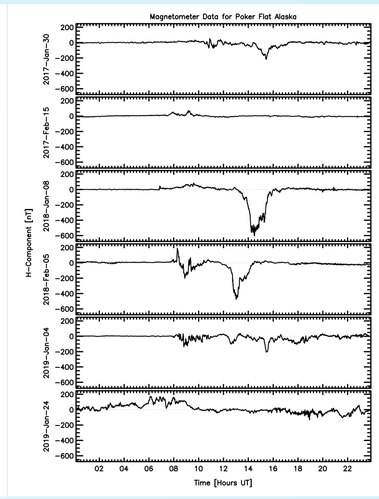

Figure7: Time series of perturbations in the H-component of magnetic fields recorded at Poker Flat Alaska for the stalled events during six days.

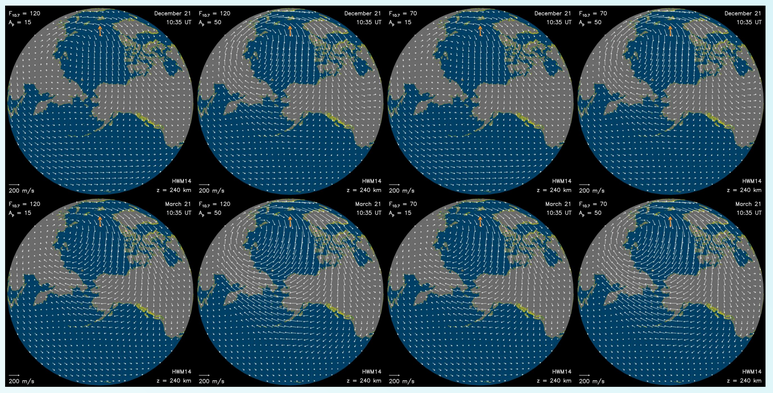

Figure 8: HWM14 wind plots for December solstice and March equinox under different conditions. HWM14 results are dominated by SDI data. However, stalling doesn’t appear in HWM14 as suddenly as our results show.

Events	Date	f10.7	Three hourly K-Indices							
			00:00-03:00	3:00-06:00	06:00-09:00	09:00-12:00	12:00-15:00	15:00-18:00	18:00-21:00	21:00-24:00
Stalled	1/30/2017	74.7	1	1	1	1	2	2	1	3
	2/15/2017	73	0	0	1	1	1	1	1	1
	1/8/2018	68	0	0	3	1	4	3	2	2
	2/5/2018	72	3	2	2	2	3	2	1	1
	1/4/2019	69.1	1	1	1	2	2	3	3	3
	1/24/2019	70.2	4	3	4	2	1	3	4	5
Emergent	1/18/2017	76.1	1	3	3	3	3	4	4	4
	2/1/2017	73.9	5	4	3	3	4	5	3	5
	12/28/2018	67	4	4	5	3	4	3	4	3
	12/29/2018	66.7	3	3	3	2	3	2	2	2
	2/1/2019	70	3	4	3	2	3	3	3	4
	3/1/2019	68.7	4	5	3	3	3	4	4	4

Table 1: Table showing the F10.7 solar radio flux data and three hourly K-indices for the observation days.

Conclusions

The data show that stalling of the cross-polar jet is most strongly controlled by season, with stalling being far more likely during deep winter, when the polar thermosphere is least exposed to sunlight, and ion densities are lowest. The next strongest control is due to magnetic activity: the jet is less likely to stall when auroral and magnetic conditions are disturbed or active, so that ion-drag drives a stronger and more dominant cross-polar jet. Perhaps surprisingly, the solar F10.7 index has least influence. This behavior is also confirmed by the HWM14 wind model, which is itself based on observations.